第 32 卷第 6 期 上 海 海 洋 大 学 学 报 Vol.32, No.6
2023 年 11 月 JOURNAL OF SHANGHAI OCEAN UNIVERSITY Nov., 2023

文章编号：1674-5566(2023)06-1099-10 DOI:10.12024/jsou.20230504200

基于Minitab软件的速冻机内圆漏斗喷嘴结构优化

谢　晶[1,2,3,4]，郭珍权[1]，柳雨嫣[1]，王金锋[1]，杨晓燕[5]，刘彦岑[1]

（1. 上海海洋大学 食品学院，上海　201306；2. 上海冷链装备性能与节能评价专业技术服务平台，上海　201306；3. 食品科学与工程国家级实验教学示范中心（上海海洋大学），上海　201306；4. 上海水产品加工及贮藏工程技术研究中心，上海　201306；5. 四方科技集团有限公司，江苏 南通　226371）

摘　要：为了增强冲击式速冻机内的传热强度和均匀性，本文以冲击式速冻机试验台为依托，提出了一种新型喷嘴结构——圆漏斗喷嘴。在该试验台被试验验证可靠的基础上，利用数值模拟技术对该试验台流场进行了模拟计算，利用Minitab软件中的Plackett-Burman设计从圆漏斗喷嘴出口直径D_E、漏斗宽度L_3、漏斗高度L_1、射流高度L_2、喷嘴排数N、喷嘴间隙S和喷嘴到钢带的距离H等7个因素中得到漏斗宽度、射流高度和喷嘴排数等3个因素为影响钢带表面努塞尔数和传热均匀度的显著性因素，然后利用Box-Behnken设计，建立3个显著性因素与钢带表面平均努塞尔数Nu_{ave}和传热均匀指标η等2个响应值之间的数学模型，确定喷嘴最佳的结构参数。结果表明：最佳结果参数为漏斗宽度17 mm、射流高度50 mm、喷嘴排数为3；在此条件下钢带表面Nu_{ave}为448.68、传热均匀指标为0.232 9，通过数值模拟得到的值与方程预测值总体吻合，说明优化得到的圆漏斗喷嘴的新型结构参数能够使速冻机的速冻效率达到最佳。

关键词：速冻机；喷嘴；努塞尔数；传热均匀度；结构优化

中图分类号：TH 122　　**文献标志码**：A

冲击射流能大大提高停滞区域的传热强度，被广泛用于造纸、冶金、食品速冻等领域[1-4]。对于速冻机，影响目标表面传热特性的主要因素是喷嘴到目标表面垂直方向上的绝对速度[5]。已有很多文献通过改变喷嘴几何形状来提高喷嘴到目标表面垂直方向上的绝对速度，进而提高冲击射流的传热特性。HE等[6]发现在喷嘴到钢带的距离与等效喷嘴直径的比值（H/D_E）为2时，3个小圆孔构造的叶形喷嘴结构的目标表面努塞尔数比单个圆孔喷嘴结构的高10%。REODIKAR等[7]研究了圆形、椭圆形、正方形和三角形喷嘴对目标表面传热特性的影响。其中圆形喷嘴的停滞点努塞尔数最高，而椭圆形喷嘴的停滞点努塞尔数最小。BHAPKAR等[8-9]指出当喷嘴到钢带的距离与等效喷嘴直径的比值（H/D_E）为6时，与圆形、方形以及矩形孔口相比，椭圆形喷嘴的传热系数最高。当H/D_E>6时，圆形和方形喷嘴的传热系数高于椭圆形和矩形喷嘴。LEE等[10]研究了相同长轴不同纵横比的椭圆形喷嘴的传热特性，当喷嘴到钢带的距离与等效喷嘴直径的比值（H/D_E）小于6时，椭圆形喷嘴的传热率比圆形喷嘴高15%。当椭圆喷嘴纵横比AR=3时，椭圆喷嘴具有最大的传热系数。从上述研究可以得出，喷嘴几何形状会影响冲击射流的换热强度，但大部分研究主要集中于分析目标表面上的Nu数大小，很少有研究关注目标表面上的传热均匀性，对于速冻机而言，传热均匀性是衡量冲击射流换热特性的一个重要指标[11-12]，传热均匀性会直接影响冻结食品的品质[13-14]。ATTALLA等[15]研究了圆形和方形喷嘴下目标表面的平均努塞尔数和传热均匀性，发现圆形喷嘴下的平均努塞尔数比方形喷嘴下的平均努塞尔数高约8.26%，而方形喷

收稿日期：2023-05-29　　**修回日期**：2023-09-20

基金项目：国家“十三五”重点研发项目（2016YFD0400303）；上海市科学技术委员会平台能力建设项目（16DZ2280300）；上海市科学技术委员会公共服务平台建设项目（17DZ2293400）

作者简介：谢　晶（1968—），女，教授，博士生导师，研究方向为制冷及低温工程，食品冷冻冷藏技术。E-mail: jxie@shou.edu.cn

通信作者：王金锋，E-mail：jfwang@shou.edu.cn

嘴的传热均匀性比圆形喷嘴高约10.45%。

Minitab软件在试验设计、质量控制、管理和科研等领域均有广泛应用[16]。Plackeet-Burman设计可以从多个影响因素中筛选出影响最显著的3个因素[17]。Box-Benhnken设计可以通过较少试验次数确定最优的设计参数组合,并得到各个因素与目标对象的函数关系及曲面图[18]。

谢晶等[19]证明了在冷却空气质量流量相同的情况下,圆漏斗喷嘴相比于圆形和椭圆形喷嘴具有更好的传热强度和传热均匀性。本文以速冻试验台的计算机模型为依托,以钢带表面平均努塞尔数 Nu_{ave} 和传热均匀性指标 η 为速冻机传热强度和均匀性的体现指标,平均努塞尔数越大,代表钢带表面换热强度越大,传热均匀性指标越小,表明钢带表面传热越均匀,首先利用Minitab软件中Plackeet-Burman设计在圆漏斗喷嘴出口直径、漏斗宽度、漏斗高度、射流高度、喷嘴排数、喷嘴间隙和喷嘴到钢带的距离等7个因素中筛选出显著性因素,然后利用Box-Benhnken得到钢带表面平均努塞尔数和传热均匀性指标与显著性因子之间的函数关系,找到使钢带表面具有更高的传热强度和更好的传热均匀性的圆漏斗喷嘴新型结构参数,以期为上下冲击式新型速冻机的优化设计提供理论依据。

1 数值模拟模型

1.1 速冻试验台计算机模型

参照南通公司的冲击式速冻机,建立速冻试验台和圆漏斗喷嘴孔板的计算机模型,如图1所示,离心风机将冷却空气送入静压箱内,通过钢带上方的孔板喷出,并向钢带一侧的冷空气出风口排出静压箱尺寸为300 mm×300 mm×500 mm,孔板尺寸为300 mm×300 mm×2 mm,此结构尺寸下该试验台内部流场变化与气流冲击式速冻机内流场变化一致[19]。图2为圆漏斗喷嘴孔板模型。图3为圆漏斗喷嘴结构参数模型。

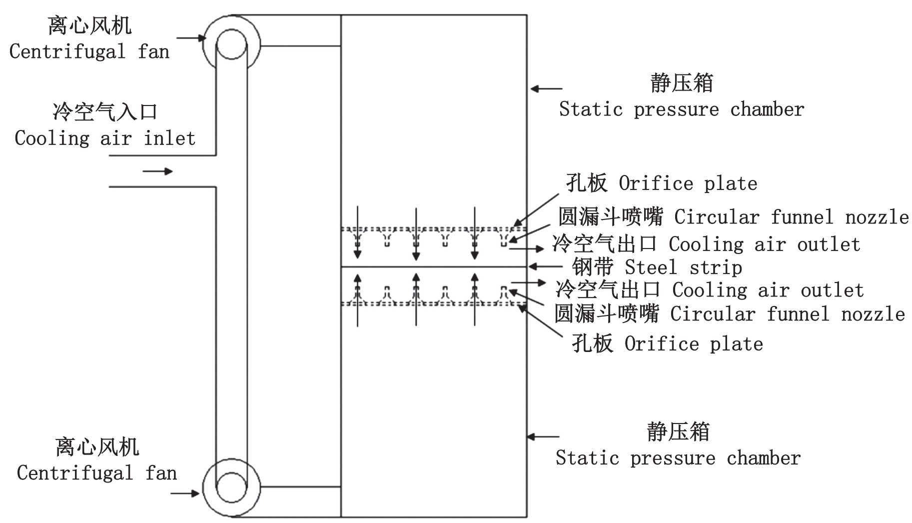

图1 冲击式速冻实验台模型

Fig. 1 Model of impacting freezing experiment table

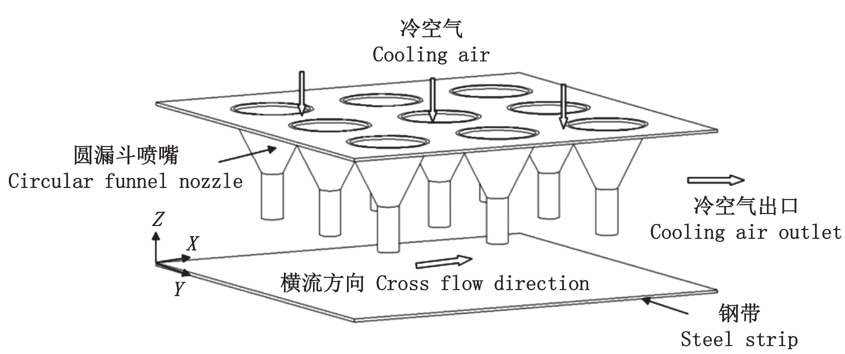

图2 圆漏斗喷嘴孔板模型

Fig. 2 Circular funnel nozzle of orifice plate model

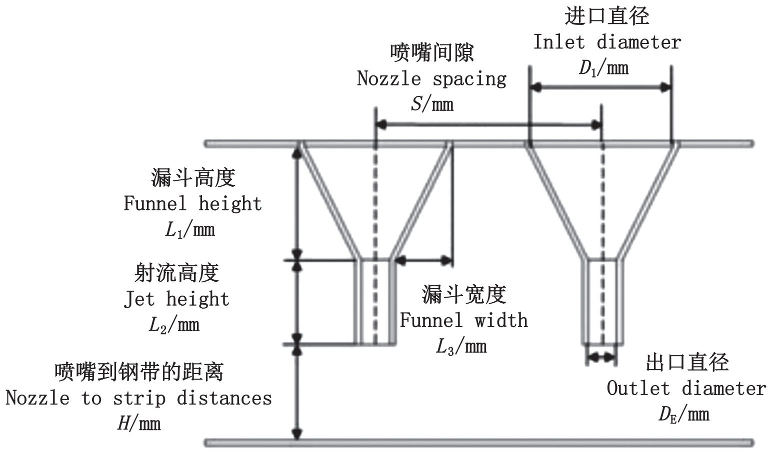

图3　圆漏斗相关参数模型

Fig. 3　Circular funnel related parameter model

1.2　网格划分

采用非结构网格对模型的计算域进行离散化处理,将圆漏斗喷嘴处的网格适当进行加密处理[20-21],圆漏斗喷嘴处加密网格最小尺寸为0.326 9 mm。整个计算域节点个数为438 358,网格单元数为1 627 915,由于圆漏斗喷嘴处为圆形,因此圆漏斗喷嘴处理结果如图4所示。

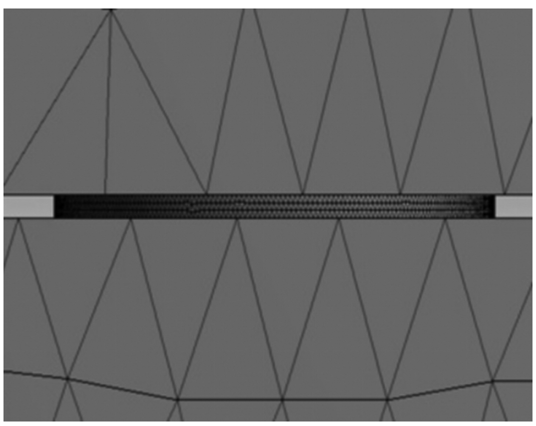

图4　圆漏斗喷嘴处网格加密

Fig. 4　Grid refinement at the circular funnel nozzle

1.3　模拟方程及边界条件设置

本次模拟的流体为空气,进行了下列假设:(1)静压箱壁面为绝热壁面[22];(2)空气为不可压缩流体[23-24];(3)模型在正常运行过程中,冲击式速冻试验台内部的流场视为稳态[25]。

本模型内部为有限空间的强制对流换热,流体的雷诺数$Re>10^6$,流体完全处于湍流状态,故本模型采用k-ε湍流模型[26]。模拟对象涉及到流动、热质守恒,因此需结合三维连续性方程、动量方程、能量方程、湍动动能k方程及湍流耗散ε方程联合求解[27]。

参考王金锋等[28]的试验方法并稍作修改,以冷却空气出入口压强差为动力,将规定流量的冷空气冲击到钢带表面,加快钢带上物体的温度降低,实现速冻效果。

1.4　参数的定义和模型的可行性验证

钢带表面平均努塞尔数Nu_{ave}定义为整个钢带表面努塞尔数的平均值。

钢带表面传热均匀指标η定义为钢带表面局部努塞尔数的标准差σ_{Nu}与钢带表面平均努塞尔数Nu_{ave}的比值[29-31],η值代表了钢带表面各个位置Nu数的差异性,η值越小,钢带表面传热越均匀,其计算公式:

$$\eta = \frac{\sigma_{Nu}}{Nu_{ave}} \tag{1}$$

谢晶等[19]试验测量了该模型每列喷嘴出口Z方向的绝对速度,将数值模拟结果与试验测量结果进行对比,两者的误差为2.83%~4.95%,可以得出对于冲击式速冻试验台的数值模拟较可靠[32]。

2　试验设计及结果

2.1　Plackett-Burman设计及结果

Plackett-Burman设计可以用最少的试验次数得到使因素的主效应最精确的估计,适用于从多个考察因素中高效地筛选出重要因素,为后续研究提供理论依据[33]。对出口直径、漏斗宽度、漏斗高度、射流高度、喷嘴排数、喷嘴间隙、喷嘴到钢带的距离等7个因素进行考察,采用试验次数为12的设计,每个因素取-1和+1两个水平,响应

值为钢带表面的平均努塞尔数(Y)。进行单因素试验,选择其中一个因素作为自变量,其余6个因素取1个适当的定值,以钢带表面Nu_{ave}数和传热均匀指标作为因变量,得到自变量的取值范围,使钢带表面具有更强的传热强度和更好的传热均匀性。改变自变量,重复单因素试验,最终得到7个因素的取值范围,Plackett-Burman试验设计参数和水平见表1,试验设计及结果见表2。7个因素对考察指标影响的次序见图5。由表1和图5可知,因素C、D、E效应显著,可作为进一步优化的因素。因素A、B、F、G效应不显著,对试验结果影响不大,在下一步研究中,取中间水平即可,对影响效果不做分析[34]。

2.2 Box-Benhnken设计及结果

以钢带表面Nu_{ave}数和传热均匀指标η为响应值,以漏斗宽度、射流高度、喷嘴排数为因变量,设计三因素三水平响应面分析试验,共17个试验点,试验因素水平如表3所示。

表1 Plackett-Burman试验设计参数和水平
Tab. 1 Parameters and levels of Plackett-Burman tests

因素 Variables	代号 Symbols	水平 Level −1	水平 Level +1
出口直径 Outlet diameter D_E/mm	A	35	45
漏斗高度 Funnel height L_1/mm	B	30	50
射流高度 Jet height L_2/mm	C	30	50
漏斗宽度 Funnel width L_3/mm	D	10	20
喷嘴排数 Nozzle Number N	E	2	3
喷嘴间隙 Nozzle spacing S/mm	F	90	95
喷嘴到钢带的距离 Nozzle-to-surface Distance H/mm	G	10	20

表2 Plackett-Burman试验设计及结果
Tab. 2 Design and results of Plackett-Burman tests

序号 Number	A	B	C	D	E	F	G	Y
1	−1	−1	−1	−1	−1	−1	−1	298.87
2	1	1	−1	−1	−1	1	−1	340.29
3	1	1	−1	1	1	−1	1	426.64
4	1	−1	1	1	−1	1	1	378.81
5	−1	1	−1	1	−1	−1	1	325.36
6	−1	−1	−1	1	1	1	−1	433.02
7	−1	1	1	−1	−1	1	1	316.81
8	1	1	1	−1	1	−1	−1	438.24
9	1	−1	−1	−1	1	1	1	398.97
10	−1	−1	1	−1	1	−1	1	425.67
11	1	−1	1	1	−1	−1	−1	342.26
12	−1	1	1	1	1	1	−1	433.71

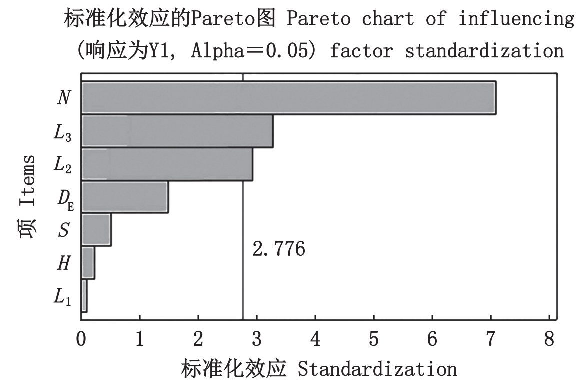

图5 影响因素标准化的帕拉图
Fig. 5 Pareto chart of influencing factor standardization

表3 响应面试验设计因素与水平
Tab. 3 Factors and levels used in response surface experiments

水平 Level	因素 Factors: X_1 漏斗宽度 L_3 Funnel width/mm	X_2 射流高度 L_2 Jet height/mm	X_3 喷嘴排数 N Nozzle number
−1	10	30	1
0	15	40	2
1	20	50	3

Box-Behnken设计试验方案及结果如表4所示,对表4数据进行多元二次回归拟合,得到二阶多项式方程:

表4 Box-Behnken设计试验方案及结果
Tab. 4 Box-Behnken design with experimental results

序号 Number	X_1-L_3	X_2-L_2	X_3-N	Y_1-Nu_{ave}	Y_2-η
1	0	0	0	344.96	0.394 5
2	0	−1	1	440.89	0.294 6
3	0	0	0	341.28	0.371 2
4	0	0	0	342.84	0.369 9
5	0	0	0	343.75	0.384 7
6	0	1	−1	206.66	0.547 0
7	0	−1	−1	201.32	0.561 8
8	−1	−1	0	340.71	0.404 7
9	−1	0	1	431.21	0.243 4
10	1	1	0	342.55	0.387 8
11	0	0	0	338.36	0.345 5
12	1	0	−1	203.28	0.626 8
13	1	0	1	451.19	0.264 1
14	−1	1	0	334.68	0.375 7
15	1	−1	0	349.37	0.383 3
16	−1	0	−1	202.59	0.535 0
17	0	1	1	449.21	0.232 1

$$Y_1=342.20+4.65X_1+0.10X_2+119.83X_3-0.20X_1X_2+4.82X_1X_3+0.74X_2X_3-1.41X_1^2+1.04X_2^2-18.72X_3^2$$

$$Y_2=0.37+0.013X_1-0.013X_2-0.15X_3+8.375\times10^{-3}X_1X_2-0.018X_1X_3-0.012X_2X_3+0.012X_1^2+3.132\times10^{-3}X_2^2+0.033X_3^2$$

表5显示了模型的方差分析,Y_1和Y_2模型的P均小于0.000 1,达到了极显著水平,失拟项的P均大于0.05,无显著性差异,这说明Y_1和Y_2模型能充分反映各个因素分别与两个响应值之间的关系[35]。Y_1和Y_2模型的决定系数R^2分别为0.999 0和0.989 4,校正决定系数R^2_{ADj}分别为0.997 6和0.983 0,与对应的R^2值都比较接近,说明Y_1和Y_2模型拟合效果都较好[36]。本试验Y_1和Y_2模型所得CV分别为1.25%和5.21%,均小于10%,Y_1和Y_2模型信噪比分别为78.025和19.795,均大于4,视为合理[37]。综上所述,回归模型可以对钢带表面Nu_{ave}和传热均匀指标结果进行分析和预测。

表5　回归方程方差分析

Tab. 5　Analysis of variances for the developed regression equation

方差来源 Source		平方和 Sum of squares	自由度 Degrees of freedom	均方 Mean square	F	P	显著性 Significance
模型 Model	Y_1	$1.166\ 4\times10^5$	9	$1.296\ 0\times10^4$	746.733 4	< 0.000 1	**
	Y_2	0.201 2	9	0.022 4	37.055 1	< 0.000 1	**
X_1	Y_1	172.980 0	1	172.980 0	9.966 4	0.016 0	*
	Y_2	0.001 3	1	0.001 3	2.206 9	0.181 0	
X_2	Y_1	0.082 0	1	0.082 0	0.004 7	0.947 1	
	Y_2	0.001 3	1	0.001 3	2.147 5	0.186 2	
X_3	Y_1	$1.148\ 8\times10^5$	1	$1.148\ 8\times10^5$	6 618.729 1	< 0.000 1	**
	Y_2	0.191 1	1	0.191 1	316.771 4	< 0.000 1	**
X_1X_2	Y_1	0.156 0	1	0.156 0	0.009 0	0.927 1	
	Y_2	0.000 3	1	0.000 3	0.465 1	0.517 2	
X_1X_3	Y_1	93.026 0	1	93.026 0	5.359 8	0.053 8	
	Y_2	0.001 3	1	0.001 3	2.095 1	0.191 0	
X_2X_3	Y_1	2.220 1	1	2.220 1	0.127 9	0.731 1	
	Y_2	0.000 6	1	0.000 6	0.943 0	0.363 9	
X_1^2	Y_1	8.388 8	1	8.388 7	0.483 3	0.509 3	
	Y_2	0.000 6	1	0.000 6	0.936 4	0.365 4	
X_2^2	Y_1	4.562 9	1	4.562 9	0.262 9	0.623 9	
	Y_2	$4.131\ 6\times10^{-5}$	1	$4.131\ 6\times10^{-5}$	0.068 5	0.801 1	
X_3^2	Y_1	1 475.372 5	1	1 475.372 5	85.005 3	< 0.000 1	**
	Y_2	0.004 5	1	0.004 5	7.410 1	0.029 7	*
残差 Residual	Y_1	121.493 7	7	17.356 2			
	Y_2	0.004 2	7	0.000 6			
失拟项 Lack of fit	Y_1	93.896 0	3	31.298 7	4.536 4	0.089 1	
	Y_2	0.002 9	3	0.000 1	2.781 9	0.174 1	
误差项 Pure error	Y_1	27.597 7	4	6.899 4			
	Y_2	0.001 4	4	0.000 3			
总和 Cor total	Y_1	$1.167\ 7\times10^5$	16				
	Y_2	0.205 4	16				
Y_1: R^2=0.999 0, R^2_{ADj}=0.997 6; Y_2: R^2=0.989 4, R^2_{ADj}=0.983 0							

注:*.P<0.05,差异显著;**.P<0.01,差异极显著。

Notes: *.P<0.05, significant difference; **.P<0.01, The difference is extremely significant.

回归方程各项方差分析中F值的大小可以判断出自变量对因变量影响的大小[38],因此由表5可得各因素对钢带表面Nu_{ave}和传热均匀性指标η影响的主次顺序为$X_3>X_1>X_2$。模型中X_3和X_3^2

对钢带表面 Nu_{ave} 数的影响达到极显著水平($P<0.01$),X_1 对钢带表面 Nu_{ave} 数的影响达到显著水平($P<0.05$),X_1X_3 和 X_2X_3 对钢带表面 Nu_{ave} 数的影响较大。模型中 X_3 对钢带表面传热均匀性指标 η 的影响达到极显著水平($P<0.01$),X_1X_3 和 X_2X_3 对钢带表面 Nu_{ave} 数的影响较大,X_3^2 对钢带表面传热均匀性指标 η 的影响达到显著水平($P<0.05$)。

响应面分析图是响应值对各自变量 X_1、X_2 和 X_3 所形成的三维曲面图,当其他因素不变时,响应面分析图反映了两两交互项对响应值的影响,响应面走势越陡,说明该自变量对响应值的影响越大,反之说明该自变量对响应值的影响越小[39-40]。各因素交互作用对钢带表面 Nu_{ave} 数和传热均匀指标 η 的影响如图6和图7所示,在交互影响中,漏斗宽度和喷嘴排数(图6b和图7b)和射流高度和喷嘴排数(图6c和图7c)之间交互作用均最为明显,这与方差分析的结果一致。

2.3 试验结果与响应面分析图的讨论

经过试验得到圆漏斗喷嘴的3个显著性因素,后续使用Box-Behnken设计试验以漏斗宽度、射流高度、喷嘴排数3个因素为因变量,钢带表面 Nu_{ave} 数和传热均匀指标为响应值,得到了钢带表面 Nu_{ave} 数和传热均匀指标的二阶多项式方程。对响应面分析图进行钢带表面传热强度和传热均匀性的分析,由图6b和图6c可知,当喷嘴排数为3时,钢带表面 Nu_{ave} 数最大,传热强度最大,由图7b和图7c可知,随着喷嘴排数的增加,传热均匀指标会减小,传热均匀性更好,因此喷嘴排数的最佳参数为3。由图6a、图6c和图7c可知,射流高度的取值在这3种情况下对响应值并无明显影响,再分析图7a可知,射流高度由30 mm增大到50 mm,钢带传热均匀指标会随之减小,钢带表面传热均匀性更好,综合分析可得射流高度的最佳参数为50 mm。将确定好的射流高度最佳参数和喷嘴排数最佳参数代入钢带表面 Nu_{ave} 数和传热均匀指标的二阶多项式方程,使其变成以漏斗宽度为唯一变量的一元二次方程,考虑实际结构的情况下,漏斗宽度应取整数,解钢带表面 Nu_{ave} 数和传热均匀指标的一元二次方程得到在漏斗宽度为17 mm时,钢带表面 Nu_{ave} 数最高,传热强度最大;传热均匀指标最小,传热均匀性最好。

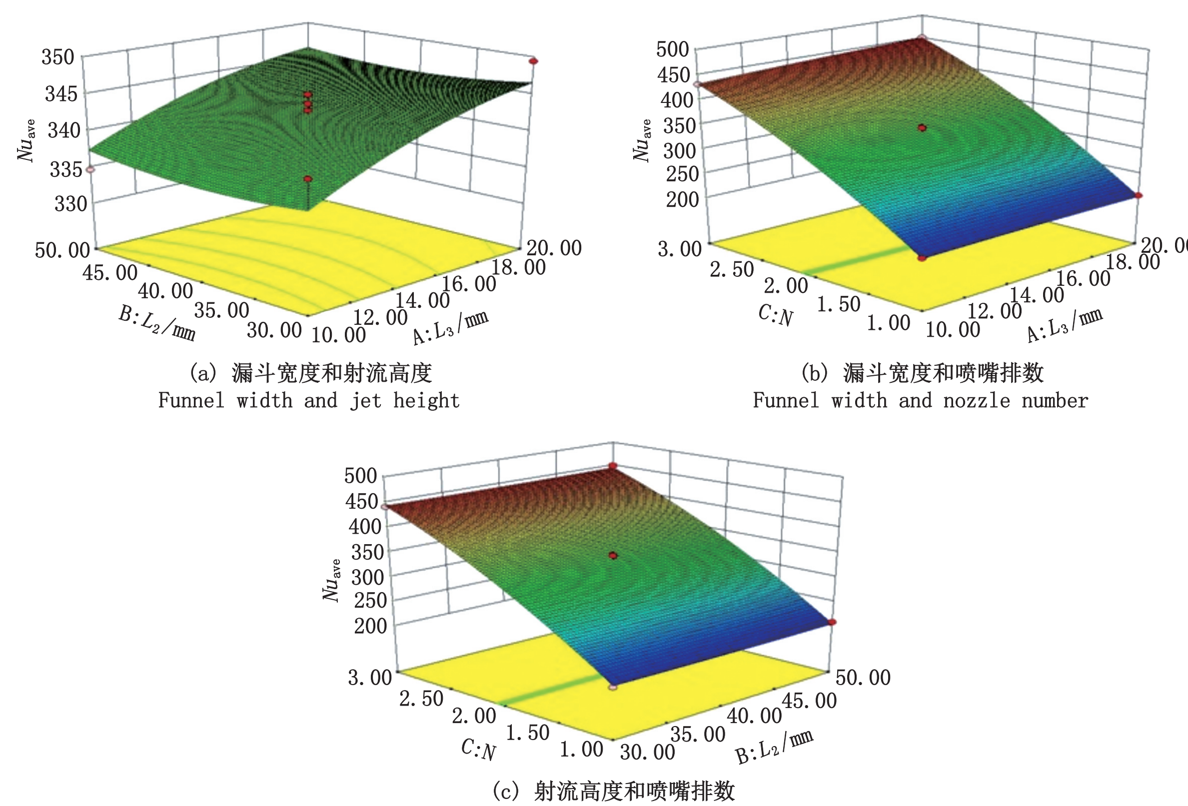

(a) 漏斗宽度和射流高度
Funnel width and jet height

(b) 漏斗宽度和喷嘴排数
Funnel width and nozzle number

(c) 射流高度和喷嘴排数
Jet height and nozzle number

图6 对钢带表面 Nu_{ave} 数影响的响应面图

Fig. 6 Response surface graphs showing the effect of average Nusselt number on steel strip

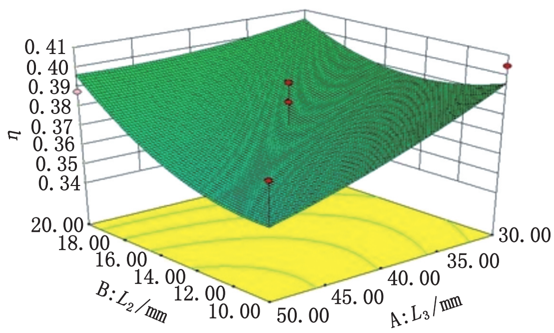

(a) 漏斗宽度和射流高度
Funnel width and jet height

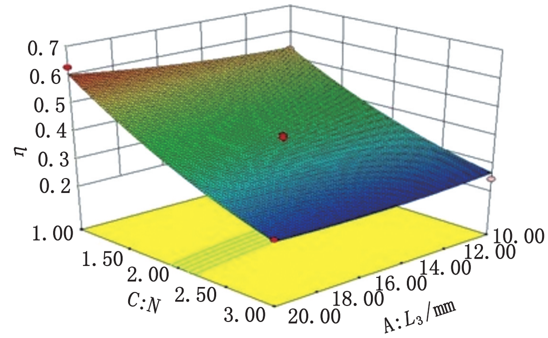

(b) 漏斗宽度和喷嘴排数
Funnel width and nozzle number

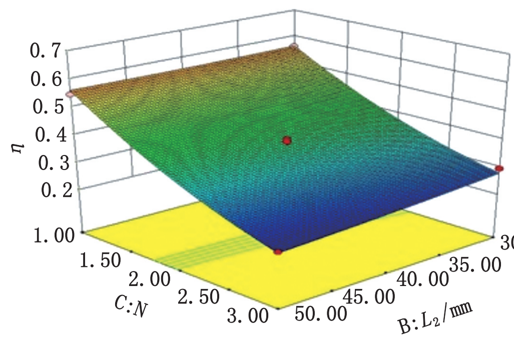

(c) 射流高度和喷嘴排数
Jet height and nozzle number

图 7　对钢带表面传热均匀性指标 η 影响的响应面图

Fig. 7　Response surface graphs showing the effect of heat transfer index uniformity index η on steel strip

当喷嘴排数由 1 变化到 3 时，钢带表面各个位置受到的冷却空气冲击更密集，温度分布以喷嘴正下方为中心，向周围扩散，温度逐步升高，喷嘴排数的增加，使得钢带表面受到的冷却空气冲击更均匀，钢带表面各点温度差减小，传热更均匀，并且，由于冷却空气冲击更密集，使得钢带表面平均温度更低，速冻效果更好。由响应面分析图可知，射流高度对钢带表面 Nu_{ave} 数影响不大，但是射流高度的增加，可以加剧冷却空气在冲击钢带表面过程中的扩散，使钢带表面冷却空气分布更均匀。综上所述，圆漏斗喷嘴结构的最佳工艺参数为漏斗宽度 17 mm、射流高度 50 mm、喷嘴排数 3，将这些参数代入拟合方程，计算得到钢带表面 Nu_{ave} 数为 448.68，传热均匀指标为 0.232 9。在此条件下经过数值模拟得到的钢带表面 Nu_{ave} 数为 448.93，传热均匀指标为 0.233 1，与预测值总体吻合，说明模型能较好地预测钢带表面 Nu_{ave} 数和传热均匀指标，优化结构条件可靠。

3　结论

本文以冲击式速冻试验台为依托，提出了一种新型圆漏斗喷嘴。以 Minitab 软件和 Box-Behnken 设计为研究工具，得出如下结论：

（1）圆漏斗喷嘴结构中对传热性能影响最大的是漏斗宽度、射流高度和喷嘴排数。

（2）只考虑显著性影响因素时，圆漏斗喷嘴最优的结构尺寸：漏斗宽度为 17 mm、射流高度为 50 mm、喷嘴排数为 3，此时钢带表面 Nu_{ave} 为 448.68，传热均匀指标为 0.232 9，传热性能最佳。

（3）将数值模拟得到的值与方程预测值进行比较得出误差值较小，证明用 Box-Behnken 设计优化钢带表面 Nu_{ave} 和传热均匀指标是可行的。

参考文献：

[1]　CHAUCHAT N, SCHALL E, MORY M, et al. Cooling of a heating cylinder by confined impacting air jets [J]. International Journal of Numerical Methods for Heat & Fluid Flow, 2016, 26(7): 2013-2032.

[2]　GRASSI C, SCHRÖTER A, GLOY Y S, et al. Reducing environmental impact in air jet weaving technology [J]. International Journal of Clothing Science and Technology, 2016, 28(3): 283-292.

[3]　WANG G, DENG Y, XU X, et al. Optimization of air jet impingement drying of okara using response surface

methodology[J]. Food Control, 2016, 59: 743-749.

[4] SINGH D, PREMACHANDRAN B, KOHLI S. Double circular air jet impingement cooling of a heated circular cylinder[J]. International Journal of Heat and Mass Transfer, 2017, 109: 619-646.

[5] 王金锋, 李文俊, 谢晶, 等. V型条缝喷嘴切割比对速冻机钢带表面换热特性的影响[J]. 食品与机械, 2018, 34(4): 94-98.
WANG J F, LI W J, XIE J, et al. Influence of V type slit nozzle cutting ratio on belt surface heat transfer characteristics of quick freezer[J]. Food & Machinery, 2018, 34(4): 94-98.

[6] HE C X, LIU Y Z. Jet impingement heat transfer of a lobed nozzle: measurements using temperature-sensitive paint and particle image velocimetry[J]. International Journal of Heat and Fluid Flow, 2018, 71: 111-126.

[7] REODIKAR S A, MEENA H C, VINZE R, et al. Influence of the orifice shape on the local heat transfer distribution and axis switching by compressible jets impinging on flat surface[J]. International Journal of Thermal Sciences, 2016, 104: 208-224.

[8] BHAPKAR U S, SRIVASTAVA A, AGRAWAL A. Acoustic and heat transfer characteristics of an impinging elliptical synthetic jet generated by acoustic actuator[J]. International Journal of Heat and Mass Transfer, 2014, 79: 12-23.

[9] BHAPKAR U S, MOHANAN S, AGRAWAL A, et al. Interferometry based whole-field heat transfer measurements of an impinging turbulent synthetic jet[J]. International Communications in Heat and Mass Transfer, 2014, 58: 118-124.

[10] LEE J, LEE S J. The effect of nozzle aspect ratio on stagnation region heat transfer characteristics of elliptic impinging jet[J]. International Journal of Heat and Mass Transfer, 2000, 43(4): 555-575.

[11] IANIRO A, CARDONE G. Heat transfer rate and uniformity in multichannel swirling impinging jets[J]. Applied Thermal Engineering, 2012, 49: 89-98.

[12] YU P P, ZHU K Q, SUN T, et al. Heat transfer rate and uniformity of mist flow jet impingement for glass tempering[J]. International Journal of Heat and Mass Transfer, 2017, 115: 368-378.

[13] LI Y L, LI F, TANG J M, et al. Radio frequency tempering uniformity investigation of frozen beef with various shapes and sizes[J]. Innovative Food Science & Emerging Technologies, 2018, 48: 42-55.

[14] LI D M, ZHU Z W, SUN D W. Effects of freezing on cell structure of fresh cellular food materials: a review[J]. Trends in Food Science & Technology, 2018, 75: 46-55.

[15] ATTALLA M, MAGHRABIE H M, QAYYUM A, et al. Influence of the nozzle shape on heat transfer uniformity for in-line array of impinging air jets[J]. Applied Thermal Engineering, 2017, 120: 160-169.

[16] CHITSAZ H, OMIDKHAH M, GHOBADIAN B, et al. Optimization of hydrodynamic cavitation process of biodiesel production by response surface methodology[J]. Journal of Environmental Chemical Engineering, 2018, 6(2): 2262-2268.

[17] AHUJA S K, FERREIRA G M, MOREIRA A R. Application of Plackett-Burman design and response surface methodology to achieve exponential growth for aggregated shipworm bacterium[J]. Biotechnology and Bioengineering, 2004, 85(6): 666-675.

[18] SABBAGH F, MUHAMAD I I, NAZARI Z, et al. From formulation of acrylamide-based hydrogels to their optimization for drug release using response surface methodology[J]. Materials Science and Engineering: C, 2018, 92: 20-25.

[19] 谢晶, 柳雨嫣, 王金锋. 喷嘴结构对气流冲击式速冻机钢带表面换热特性的影响[J]. 农业工程学报, 2018, 34(18): 292-298.
XIE J, LIU Y Y, WANG J F. Effects of nozzle structures of air impinging freezer on heat transfer characteristics of steel strip surface[J]. Transactions of the Chinese Society of Agricultural Engineering, 2018, 34(18): 292-298.

[20] XU L, LAN J, MA Y H, et al. Numerical study on heat transfer by swirling impinging jets issuing from a screw-thread nozzle[J]. International Journal of Heat and Mass Transfer, 2017, 115: 232-237.

[21] GUAN T, ZHANG J Z, SHAN Y. Convective heat transfer by a row of tab-excited impinging jets on a wedge-shaped concave surface[J]. International Journal of Thermal Sciences, 2016, 100: 37-53.

[22] CHEN L L, BRAKMANN R G A, WEIGAND B, et al. Experimental and numerical heat transfer investigation of an impingement jet array with V-ribs on the target plate and on the impingement plate[J]. International Journal of Heat and Fluid Flow, 2017, 68: 126-138.

[23] ZHU X W, ZHU L, ZHAO J Q. An in-depth analysis of conjugate heat transfer process of impingement jet[J]. International Journal of Heat and Mass Transfer, 2017, 104: 1259-1267.

[24] SINGH D, PREMACHANDRAN B, KOHLI S. Effect of nozzle shape on jet impingement heat transfer from a circular cylinder[J]. International Journal of Thermal Sciences, 2015, 96: 45-69.

[25] LI Y M, LI B K, QI F S, et al. Flow and heat transfer of parallel multiple jets obliquely impinging on a flat surface[J]. Applied Thermal Engineering, 2018, 133: 588-603.

[26] HOSAIN M L, BEL FDHILA R, DANERYD A. Heat transfer by liquid jets impinging on a hot flat surface[J]. Applied Energy, 2016, 164: 934-943.

[27] HOU Y, TAO Y J, HUAI X L, et al. Numerical simulation of multi-nozzle spray cooling heat transfer[J]. International Journal of Thermal Sciences, 2018, 125: 81-88.

[28] 王金锋, 李文俊, 谢晶, 等. 两种喷嘴结构对冲击式速冻机流场及换热特征的影响[J]. 食品与机械, 2017, 33(12): 80-85, 90.
WANG J F, LI W J, XIE J, et al. Influence of two ddifferent nnozzle fforms on the flow ffield and heat transferring characteristics of qquick freezer[J]. Food & Machinery, 2017, 33(12): 80-85, 90.

[29] SUBASI A, SAHIN B, KAYMAZ I. Multi-objective optimization of a honeycomb heat sink using Response Surface Method[J]. International Journal of Heat and Mass Transfer, 2016, 101: 295-302.

[30] WEN Z X, HE Y L, MA Z. Effects of nozzle arrangement on uniformity of multiple impinging jets heat transfer in a fast cooling simulation device[J]. Computers & Fluids, 2018, 164: 83-93.

[31] 马朝, 严超, 曹学伟, 等. 阵列空气射流传热均匀性问题的数值研究[J]. 工程热物理学报, 2016, 37(11): 2378-2384.
MA Z, YAN C, CAO X W, et al. Numerical study on array air jet heat transfer uniformity[J]. Journal of Engineering Thermophysics, 2016, 37(11): 2378-2384.

[32] 陈黎卿, 张栋, 陈无畏. 基于流固耦合的分动器齿轮两相流动数值模拟与试验[J]. 农业工程学报, 2014, 30(4): 54-61.
CHEN L Q, ZHANG D, CHEN W W. Numerical simulation and test on two-phase flow inside shell of transfer case based on fluid-structure interaction[J]. Transactions of the Chinese Society of Agricultural Engineering, 2014, 30(4): 54-61.

[33] TANG X, LUO J Q, LIU F. Aerodynamic shape optimization of a transonic fan by an adjoint-response surface method[J]. Aerospace Science and Technology, 2017, 68: 26-36.

[34] DJENOUHAT M, BENDEBANE F, BAHLOUL L, et al. Optimization of methylene blue removal by stable emulsified liquid membrane using Plackett-Burman and Box-Behnken designs of experiments[J]. Royal Society Open Science, 2018, 5(2): 171220.

[35] KIM P, HABER H L, LLOYD J, et al. Optimization of thermal desorption conditions for recovering wood preservative from used railroad ties through response surface methodology[J]. Journal of Cleaner Production, 2018, 201: 802-811.

[36] KHAMPARIA S, JASPAL D. Study of decolorisation of binary dye mixture by response surface methodology[J]. Journal of Environmental Management, 2017, 201: 316-326.

[37] SHABAN A, SHALABY M A. Modeling and optimizing of variance amplification in supply chain using response surface methodology[J]. Computers & Industrial Engineering, 2018, 120: 392-400.

[38] GHARAIBEH M A. Reliability analysis of vibrating electronic assemblies using analytical solutions and response surface methodology[J]. Microelectronics Reliability, 2018, 84: 238-247.

[39] GUPTA V K, FAKHRI A, AGARWAL S, et al. Synthesis of MnO_2/cellulose fiber nanocomposites for rapid adsorption of insecticide compound and optimization by response surface methodology[J]. International Journal of Biological Macromolecules, 2017, 102: 840-846.

[40] GUPTA V K, AGARWAL S, ASIF M, et al. Application of response surface methodology to optimize the adsorption performance of a magnetic graphene oxide nanocomposite adsorbent for removal of methadone from the environment[J]. Journal of Colloid and Interface Science, 2017, 497: 193-200.

Optimization of circular funnel nozzle structure in air impinging freezer by Minitab

XIE Jing[1,2,3,4], GUO Zhenquan[1], LIU Yuyan[1], WANG Jinfeng[1], YANG Xiaoyan[5], LIU Yancen[1]

(1. *College of Food Science and Technology*, *Shanghai Ocean University*, *Shanghai* 201306, *China*; 2. *Shanghai Professional Technology Service Platform on Cold Chain Equipment Performance and Energy Saving Evaluation*, *Shanghai* 201306, *China*; 3. *National Experimental Teaching Demonstration Center for Food Science and Engineering* (*Shanghai Ocean University*), *Shanghai* 201306, *China*; 4. *Shanghai Engineering Research Center of Aquatic Product Processing & Preservation*, *Shanghai* 201306, *China*; 5. *Square Technology Group Co.*, *Ltd.*, *Nantong* 226371, *Jiangsu*, *China*)

Abstract: In order to enhance the heat transfer intensity and uniformity in an air impinging freezer, an impinging freezing experimental table was designed as the research object, and a new nozzle structure—circular funnel nozzle was proposed. The numerical simulation technology was used to simulate the flow fields in the impinging freezing experimental table, which was testified by experiments. The flow medium was air, and the simulation process assumes: (1) The wall of static pressure chamber was adiabatic. (2) Air was an incompressible, homogeneous viscous fluid. (3) During the normal operation, the internal flow field of the model was regarded as steady state. The three-dimensional continuity equation, the momentum equation, the energy equation, the kinetic energy k equation and the turbulent dissipation ε equation were used. The cooling air inlet and outlet pressure were 250 Pa (P_{in}) and 0 Pa (P_{out}) respectively. For the frozen area, the cooling air inlet and outlet temperature was 230 K and 235 K. The mass flow rate at the cooling air inlet is 0.064 4 kg/s. The thermal conductivity of steel strip was 16.3 W/(m·℃). Using the Plackett-Burman design, the significant factors for the average Nusselt number on the steel strip surface were obtained from the factors of outlet diameter D_E, funnel width L_3, funnel height L_1, jet height L_2, nozzle number N, nozzle spacing S and nozzle-to-surface distance H. These significant factors were funnel width L_3, jet height L_2 and nozzle number N. The others had little effect on the average Nusselt number. So in the next study, these factors adopted the median values. Then, using the Box-Behnken design, a mathematical model between those three significant factors and the two response values which were average Nusselt number Nu_{ave} and the heat transfer uniformity index η on the steel strip surface was established to determine the optimal structural parameters. The F value in the regression equation can be used to determine the influence of the factors on the response value. Therefore, the order of the factors affecting the average Nusselt number and the heat transfer uniformity index on the steel strip surface was nozzle number>funnel width>jet height. The interaction between the funnel width and the number of nozzle rows, the jet height and the number of nozzle rows were the most significant in the response surface analysis figures, which were consistent with the results of the variance analysis. The results showed that the optimal structural parameters were funnel width L_3=17 mm, jet height L_2=50 mm, nozzle number N=3. Substituting these parameters into the second-order polynomial equation, the average Nusselt number on the steel strip surface Nu_{ave}=448.68, heat transfer uniformity index η on the steel strip surface=0.232 9. The numerical simulation value was generally consistent with the predicted value, so it was reasonable to optimize the average Nusselt number and the heat transfer uniformity index on the steel strip surface by using the Box-Behnken design.

Key words: freezer; nozzle; Nusselt number; uniformity of heat transfer; structural optimization